nature communications

Article

https://doi.org/10.1038/s41467-025-64126-2

Non-volatile tuning of cryogenic silicon photonic micro-ring modulators

Received: 16 October 2024

Accepted: 5 September 2025

Published online: 21 October 2025

Check for updates

Uthkarsh Adya[1], Sridhar Singhal[1], Rui Chen[1], I-Tung Chen[1], Sanskriti Joshi[1], Arka Majumdar[1,2], Mo Li[1,2] & Sajjad Moazeni[1]

Quantum computing, ultra-low-noise sensing, and high-energy physics experiments often rely on superconducting circuits or semiconductor qubits and devices operating at deep cryogenic temperatures (4K and below). Photonic integrated circuits and interconnects have been demonstrated for scalable communications and optical domain transduction in these systems. Due to energy and area constraints, many of these devices need enhanced light-matter interaction, provided by photonic resonators. A key challenge, however, for using these resonators is the sensitivity of resonance wavelength to process variations and thermal fluctuations. While thermo-optical tuning methods are typically employed at room temperature to mitigate this problem, the thermo-optic effect is ineffective at 4K. To address this issue, we demonstrate a non-volatile approach to tune the resonance of photonic resonators using integrated phase-change materials (PCMs) at cryogenic temperatures. In this work, we report a 10 Gb/s free-carrier dispersion based resonant photonic modulator that can be tuned in a non-volatile fashion at sub-4K temperatures using a commercial silicon photonics process. This method paves the way for realizing scalable cryogenic integrated photonics with thousands of resonant devices for quantum and high-energy physics applications.

Optical interconnects will be essential for future cryogenic quantum and classical computing as well as high-energy physics (HEP) detector systems to communicate data and control signals between room temperature (RT) and cryogenic stages[1–3]. Recent demonstrations have shown promising advantages of optical fiber links over electrical cables, including ultra-high bandwidths resulting in the ability to achieve terabits-per-second (Tb/s) data rates over long distances, minimal heat load transferred to the cryogenic stage, and negligible thermal noise[1,4,5]. The key components enabling such optical links for practical and scalable systems are cryogenic photonic resonators and resonant modulators, which offer low-voltage and energy-efficient modulation within a compact footprint[6–8]. These resonators have also been directly interfaced with superconducting qubits and circuits for electro-optical transduction[9,10].

These resonators can be fabricated using advanced silicon photonics processes provided by commercial foundries, enabling the development of large-scale, practical photonic integrated circuits (PICs)[11–13]. However, the major challenge in using photonic resonators and resonant modulators is the crucial need for controlling and tuning their resonance wavelengths[6–8,14]. This is due to the fact that the absolute resonance wavelength and the input laser wavelength of the resonator will not be exactly identical due to process variations. At RT, this challenge can be addressed by thermal tuning of the resonance, using an integrated thermo-optic phase shifter, in a closed- or open-loop fashion[14–17]. However, at cryogenic temperatures (below 4 K), the thermo-optic effect is extremely weak (silicon's thermo-optic coefficient degrades from ~10^{-4} at 300 K to ~10^{-9} at 4 K)[13,18]. Furthermore, thermo-optical phase shifters require a supply of constant DC currents

[1]Department of Electrical and Computer Engineering, University of Washington, Seattle, WA, USA. [2]Department of Physics, University of Washington, Seattle, WA, USA. e-mail: smoazeni@uw.edu

https://doi.org/10.1038/s41467-025-64126-2

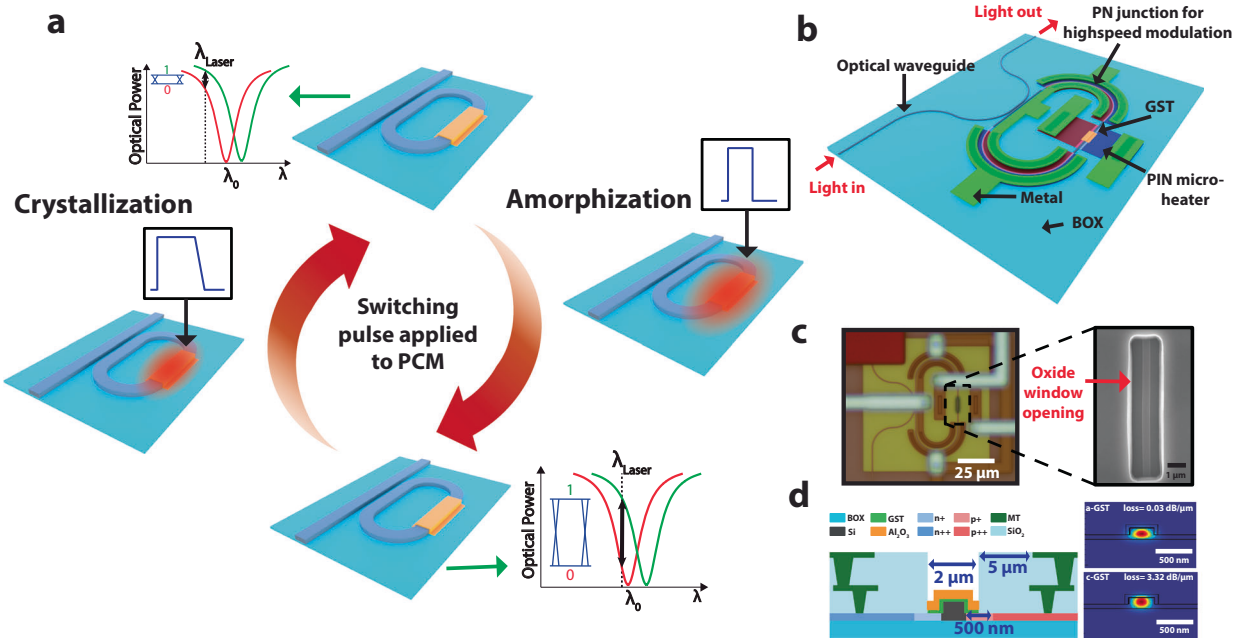

Fig. 1 | Cryogenic-compatible phase change material integrated micro-ring modulator. a The concept of tuning the micro-ring modulator (MRM) resonance in a non-volatile fashion using cryogenic phase change material (PCM), **b** Device illustration of PIN micro-heater integrated with race-track MRM, **c** Micrograph of the proposed MRM device, **d** Cross-section of PIN micro-heater and mode profile simulation with 10-nm-thick GST on the waveguide.

resulting in large power dissipation, which is undesirable in cryogenic systems due to their limited cooling power budgets. In addition, using a set of separate tunable laser sources[19] for large-scale systems with hundreds of photonic resonators is not practical. Therefore, it is crucial to develop an alternative tuning method for cryogenic photonic resonators that can provide a sufficiently large resonance tuning range (typically few-nm wavelength range equivalent to over π phase-shift) at ultra-low powers, while maintaining the compatibility with today's silicon photonic foundry process for scalability.

Several methods have been demonstrated to modulate the resonance wavelength of a photonic resonator, including opto-mechanics[20], magneto-optics[21], and electro-optical effects such as the Pockels effect[5,22–24] and the DC Kerr effect[25]. However, these optical effects are relatively weak cryogenic optical effects that are only suitable for small modulations of the resonance (typically by less than 0.1 nm perturbations). Therefore, they either require very large voltages (e.g., more than 50 V for tuning over even a small range of 1 nm resonance shift), very large device footprints (~0.4 m[22]) or consume enormous electrical power, exhibiting severe pitfalls for cryogenic applications with limited cooling power. MEMS-based[26] approaches can be a promising solution providing a large tuning range, along with a small foot-print, if integrated with cryogenic silicon photonic resonators but their volatile nature and extremely large voltage requirements (ranging from 50 to 200 V) can severely limit scalability. Moreover, none of these above approaches can be seamlessly integrated with high-speed resonant modulators as an additional resonance tuning knob. Finally, most of these methods require materials that are very challenging to integrate with the foundry silicon photonics.

In this work, we address the above-mentioned challenge by monolithic integration of non-volatile chalcogenide-based phase-change materials (PCM) with silicon photonics to tune a silicon micro-ring modulator (MRM) at sub-4 K temperatures. MRMs are one of the most promising resonant photonic modulators for realizing cryogenic optical links and transduction. In addition to enabling ultra-low-power modulation with almost 10 GHz bandwidths using the free carrier-plasma dispersion effect[6,8], MRMs naturally support wavelength division multiplexing (WDM), allowing simultaneous communication over multiple wavelengths through a single fiber. For cryogenic MRMs, the ring resonance (λ_{MRM}) needs to be precisely aligned with the laser wavelength (λ_{Laser})[6–8,14]. To achieve maximum optical modulation amplitude (OMA), λ_{MRM} must be optimally detuned from λ_{Laser} (illustrated in Fig. 1a). This type of tuning will be achieved through non-volatile programming of PCM.

The two states of PCM, amorphous or crystalline, with distinct optical properties and it can be reversibly switched using tailored heat pulses. After switching, the PCM remains in its state in a non-volatile manner, without any static power dissipation. Electrically-programmable PCM have been employed for realizing photonic switches[27,28], directional couplers[29], and optical computing[30,31] in RT. Using the prototypical PCM $Ge_2Sb_2Te_5$ (GST), we demonstrate a large resonance shift of 0.42 nm (with minor Q-factor reduction) for an MRM with a free spectral range (FSR) of 4.5 nm at 4 K temperature. The GST with 12.5 nm thickness is deposited on an 8-µm-long section of the MRM. Notably, while the PCM is programmed locally on the sub-100-µs timescale by heating the device, we demonstrate that the entire chip temperature stabilizes at the base temperature of the cryostat. This work presents the first-ever demonstration of cryogenic non-volatile photonics, where a thin film of GST is electrically switched at sub-4 K temperatures. Lastly, we will show a cryogenic optical MRM with closed-loop non-volatile tuning of resonances using GST. We report a modulation bit rate of +10 Gb/s with an extinction ratio (ER) of 4.94 dB. Our demonstration paves the way for ultra-low power and high-performance cryogenic resonant modulators beyond fabrication limitations.

Cryogenic-compatible PCM integrated micro-ring modulator

The development of promising modulators is key for enabling room-temperature to cryogenic photonic links that can help scale up many of the emerging cryogenic systems. To further extend the bandwidth of these links, wavelength division multiplexing (WDM) can be implemented using MRMs. In the case of MRMs, tuning for process variations is crucial for the performance of these modulators and also

https://doi.org/10.1038/s41467-025-64126-2

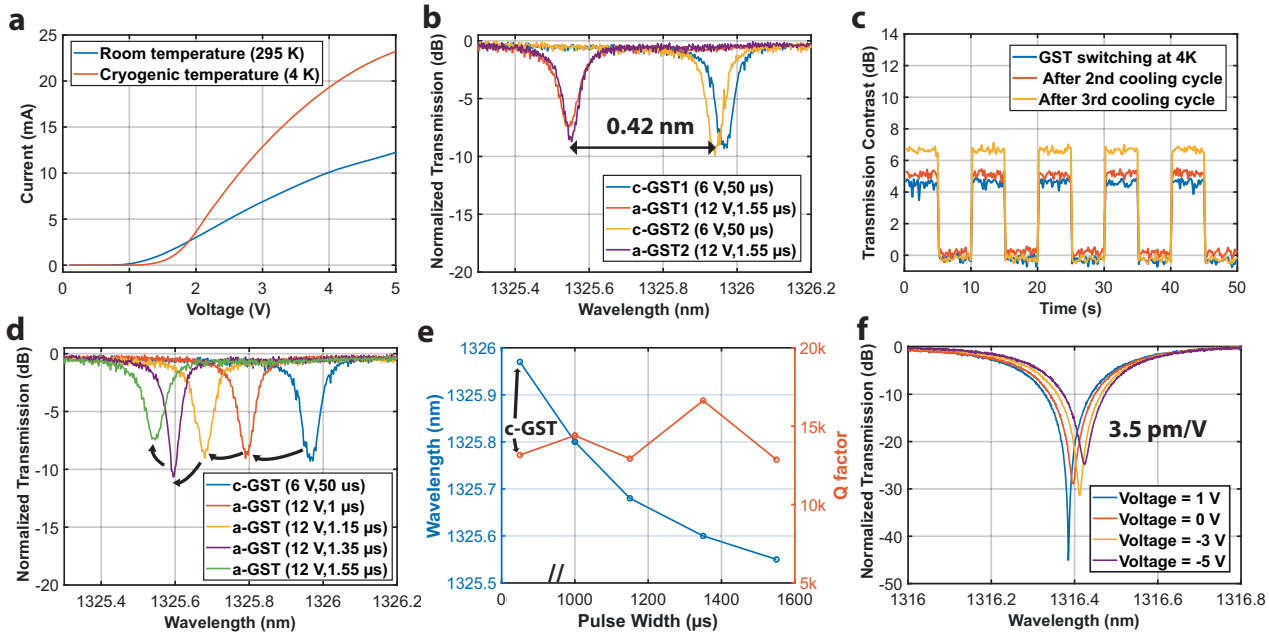

Fig. 2 | Phase change material tuning characterization. a IV characteristics of the PIN micro-heater at room temperature (RT) and 4 K, **b** Normalized transmission plot demonstrating the micro-ring modulator (MRM) phase shift induced by GST switching at 4 K, **c** Change in transmission, near resonance, over consecutive switching events over time and after repeated cooling (from RT to 4 K) of the device, **d** Multilevel switching of GST at 4 K, **e** Resonance wavelength shift of the MRM during multilevel operation, **f** Optical transmission of the MRM for various voltages applied to the PN junction for high-speed modulation.

to further extend their capabilities using WDM. Ideally, the tuning range must be the whole FSR range to ensure robust performance of the modulator over large process and temperature variations. However, in practical dense WDM (DWDM) applications, the tuning range must be sufficient to cover the typical channel spacing of 1–2 nm. Non-volatile switching in chalcogenide-based PCMs such as GST[32–34], SbS[27,35,36], and SbSe[37–40] alloys presents a promising solution for post-fabrication resonance tuning of photonic resonators, particularly for cryogenic applications. Integration of a PCM section into MRMs, with a typical modulation rate of 10 Gb/s, can provide an independent non-volatile tuning at cryogenic temperatures in addition to the modulation capability of the MRM. To achieve this, we propose a PCM-integrated racetrack MRM where the OMA can be maximized by precisely tuning the device to its "on-resonance" state, that is slightly detuned from the input laser light wavelength as depicted in Fig. 1a. Electrical programming of the PCM can be performed using a PIN (P-type, Intrinsic, N-type) diode micro-heater structure[33,41,42]. Our MRM device is designed with a section that includes this embedded PIN micro-heater, while the remaining portion of the resonator enables high-speed modulation using PN junctions based on the free carrier-plasma dispersion effect (Fig. 1b). In this work, we utilize the prototypical PCM GST due to its large optical contrast, with a typical room temperature refractive index of 6.63 + 1.55i and 4.6 + 0.34i in the crystalline and amorphous states, respectively[32]. We designed the MRM device to be in a highly over-coupled state to have a relatively low Q-factor for accommodating high electro-optical modulation bandwidths[15]. The bent regions of the racetrack MRM have a radius of 10 µm, the waveguide core was doped with the lowest (n/p) concentration, with the doping level increasing as we move further away from the core (see Supplementary Note 5). The coupler between the MRM and the bus waveguide featured a coupling gap of 350 nm and a coupling length of 2 µm. Based on FDTD simulations, this combination of gap and length was estimated to transfer ~13.75% of the power from the bus waveguide into the ring (see Supplementary Note 5). Additionally, since GST exhibits higher optical loss in its crystalline state, operating in the over-coupled regime helps ensure that switching does not cause a significant change in the transmission spectrum of the modulator.

The state of the GST can be reversibly switched by applying a tailored heat pulse that induces a microstructural phase change from the amorphous (a-GST) to crystalline (c-GST) state (the "SET" process) and vice versa (the "RESET" process)[43]. The GST film can be crystallized by maintaining the temperature above its crystallization temperature (T_c ~ 423 K[44–46]) and below its melting temperature (T_m ~ 923 K[28]). It can be switched back to the amorphous state when heated above T_m and cooled rapidly. We will study and discuss the impacts of such large temperature requirements during the programming of PCM for cryogenic photonics in Section Thermal Characterization.

Despite the significant advantages of PCM-based photonics, these materials are not currently available in any commercial silicon photonics. Previous efforts to embed PCM in silicon photonics have required custom modifications to the foundry process[37,47–49]. Recently, we demonstrated a "zero-change" post-processing methodology for back-end-of-line (BEOL) monolithic integration of GST into a commercial silicon photonics process[50]. We leveraged this approach to realize the proposed MRM devices in a commercial foundry silicon photonics platform using available doping and waveguide features of the process (see Section Methods).

Results

Cryogenic MRM characterization

First, we conducted optical measurements to validate the GST switching at cryogenic temperatures and to determine the appropriate switching pulse parameters including pulse voltages, pulse widths, and rise/fall times. We characterized the PIN micro-heater by comparing its I-V characteristics at both RT and 4 K, as shown in Fig. 2a. We observed that the current through the diode was significantly higher, and the threshold voltage was slightly elevated at 4 K, as expected due to higher mobility at 4 K[51,52]. For characterizing resonance tuning at 4 K, we utilized an MRM variant with an 8 µm oxide window opening, in which a 12.5 nm GST thin film was deposited. At 4 K, GST was amorphized by applying a 12 V pulse for 1.55 µs (switching energy = 2.09 µJ),

and crystallized by applying a 6 V pulse for 50 µs with a 36 µs falling edge (switching energy = 9.55 µJ). Figure 2b shows the normalized transmission in the O-band (1310 nm) between the two GST states, where we observed a resonance shift of 0.42 nm (for an MRM with FSR = 4.5 nm). The switching is repeatable, up to 1500 switching events (see Supplementary Note 2), and non-volatile, as demonstrated by the binary switching operation in Fig. 2c. In this experiment, the laser was tuned to a point near the resonant wavelength where sufficient transmission contrast can be observed when GST is switched. An average ER of 5 dB was measured in this binary switching experiment, not representing the full extinction of the resonator.

We repeated the binary switching measurements each time the device was brought back to RT and then cooled down to 4 K. We performed three such cool-down cycles to assess whether GST switching behavior is affected in any manner. The device consistently operated as a binary switch with only slight variations in ER, indicating that repeated cooling minimally impacts the GST switching properties. However, there is a slight degradation which we believe is due to the partial switching of GST, and can be corrected by appropriately adjusting the switching pulses. Additionally, we performed multilevel switching operations with GST, as depicted in Fig. 2d. Multilevel switching was achieved by employing pulse width modulation to tune the resonance wavelength from c-GST to a-GST in four steps. The total Q-factor of the MRM is measured to be ~13,000, and it shows minimal variation during multilevel switching, as shown in Fig. 2e. The minor intrinsic Q-factor reduction from ~45,000 in the amorphous dominant state to ~40,000 in the crystalline dominant state, suggests an excessive round-trip loss of 0.57 dB. It is also important to note that here the GST might be switching to a partially crystalline state, where the crystalline phase is dominant. This partial switching can be attributed to several factors that include ineffective heating of the full volume of GST, and thinning of the GST layer due to material reflow during the amorphization process. Moreover, the shadowing effect in oxide openings can result in a thinner-than-intended deposition of material, and the switching of PCM in the opening can cause a topographical change in the GST volume, moving the material away from the waveguide during the crystallization process[53], leading to additional thinning of the material on top of the waveguide. We believe these factors limit the device from experiencing the full extent of optical losses expected in the crystalline state of GST, as predicted by simulations. However, we benefit from this partial crystallization process as it enables multilevel switching capability, while preserving the overall Q-factor, which is crucial for fine resonance tuning of the MRM at cryogenic temperatures.

Furthermore, we characterized the free-carrier dispersion effect at 4 K (see Supplementary Note 4), and observed a resonance shift efficiency of 3.5 pm/V (Fig. 2f), similar to the RT measurements. We note that this current modulation efficiency can be improved up to 15 pm/V in this process using highly doped PN junctions[54], which leads to lower Q-factors. More advanced silicon photonics can be utilized in the future to achieve 50 pm/V modulation efficiencies[6,55].

Thermal characterization

Electro-thermal devices such as thermal phase-shifters are generally not ideal for cryogenic applications as they can exceed the cooling power budget of the cryostat (similarly true for magneto-optical photonics). The heat generated to switch the GST phase is less of a concern to the cooling power of the cryostat since the heat, produced by the short switching pulses, is only generated during the switching process and is localized within a small MRM area. However, one potential concern is heat leakage, which could affect the operation of adjacent thermal-sensitive devices such as superconducting circuits and photodetectors. To characterize the temperature stress around the device during tuning, we utilized the PN junction sections of the MRM as temperature sensors (Fig. 3b) to record temperature variations when a GST switching pulse was applied to the PIN micro-heater (Fig. 3a).

The temperature sensor was characterized by performing I-V sweeps at successive temperatures, from 4 K to 295 K, as shown in Fig. 3c. Figure 3d presents the voltage recorded across the temperature sensor as a function of temperature. After applying the pulse to the PIN micro-heater, the temperature was measured at two locations: on the same MRM device under test (DUT) as the PIN micro-heater is being programmed, and on an adjacent MRM device located 50 µm away. When the PCM switching pulse was applied, a negligible temperature rise was detected on the adjacent device that was located 50 µm away, as indicated by the blue plot in Fig. 3e, f.

In contrast, a temperature rise was observed when the PIN micro-heater and the temperature sensors were co-located at the same ring (Fig. 3a). During crystallization, the temperature rose to 120 K and dropped back to 4 K within 140 µs (Fig. 3f), while during amorphization, the temperature rose to 75 K and returned to 4 K within 60 µs (Fig. 3e). The temperature measured here will correspond to the average temperature across the ring while only the PIN micro-heater section of the MRM is switched, suggesting that the temperature rise is highly localized within the same device, returning to 4 K within a few microseconds. Moreover, the temperature rise has a negligible effect beyond 50 µm from the PIN micro-heater.

Cryogenic optical modulator with resonance tuning

Lastly, we demonstrate an optical transmitter operating at cryogenic temperatures that included the racetrack MRM for high-speed modulation, and a PCM-based closed-loop resonance tuning scheme. In this experiment, we demonstrate how non-volatile reconfiguration of the MRM's resonance via GST enables successful data modulation with maximum OMA and ER, despite initial misalignment between the laser and MRM resonance wavelengths. To characterize the modulation performance of the PCM-integrated MRM, we performed optical high-speed data transmission measurement in a 4 K cryogenic electro-optical probe station. A high-speed electrical signal was applied to the MRM's PN junctions at a data rate of 10.35 Gb/s and applied voltage levels of 0 V and −3.6 V, ensuring depletion-mode operation for high-speed data modulation[6] using a random bit pattern generator. We characterized the high-speed modulation performance of the MRM in either state of PCM. When the modulator was operated at the on-resonance point with GST in its amorphous state (λ_{MRM} = 1325.511 nm), an eye diagram was captured using an external high-speed photodetector (PD), as shown in Fig. 4b. We measured an ER of 4.94 dB and an insertion loss (IL) of 2.73 dB (OMA = 0.36). Next, the GST was switched to its crystalline state, and the laser was tuned to the new on-resonance point (λ_{MRM} = 1325.939 nm), yielding an ER of 3.81 dB and an IL of 3 dB (OMA = 0.29). This shows we can achieve a high data rate modulation regardless of the PCM state. To further contextualize the modulator performance, we have also performed additional characterization of the modulator IL, ER, and Bit Error Rate (BER) under different modulation conditions (See Supplementary Note 4).

To demonstrate the non-volatile tuning of the MRM resonance using GST, the laser wavelength was fixed at an arbitrary wavelength, around ~1325.5 nm in this case near the amorphous on-resonance point. The GST was initially set to its highest crystalline dominant state, where the laser wavelength is far off-resonance, and no eye-opening was observed on the oscilloscope. The modulator was then tuned using partial-amorphization pulses to perform multilevel switching to eventually bring the modulator closer to the on-resonance point with a closed-loop monitoring setup (see Methods). The tuning loop works based on monitoring the average optical power from the output of MRM (via a second PD and a 10/90 coupler), and locking the average optical power at the output of the modulator to ideal pre-calculated values based on initial characterizations of the MRM with a target locking range.

https://doi.org/10.1038/s41467-025-64126-2

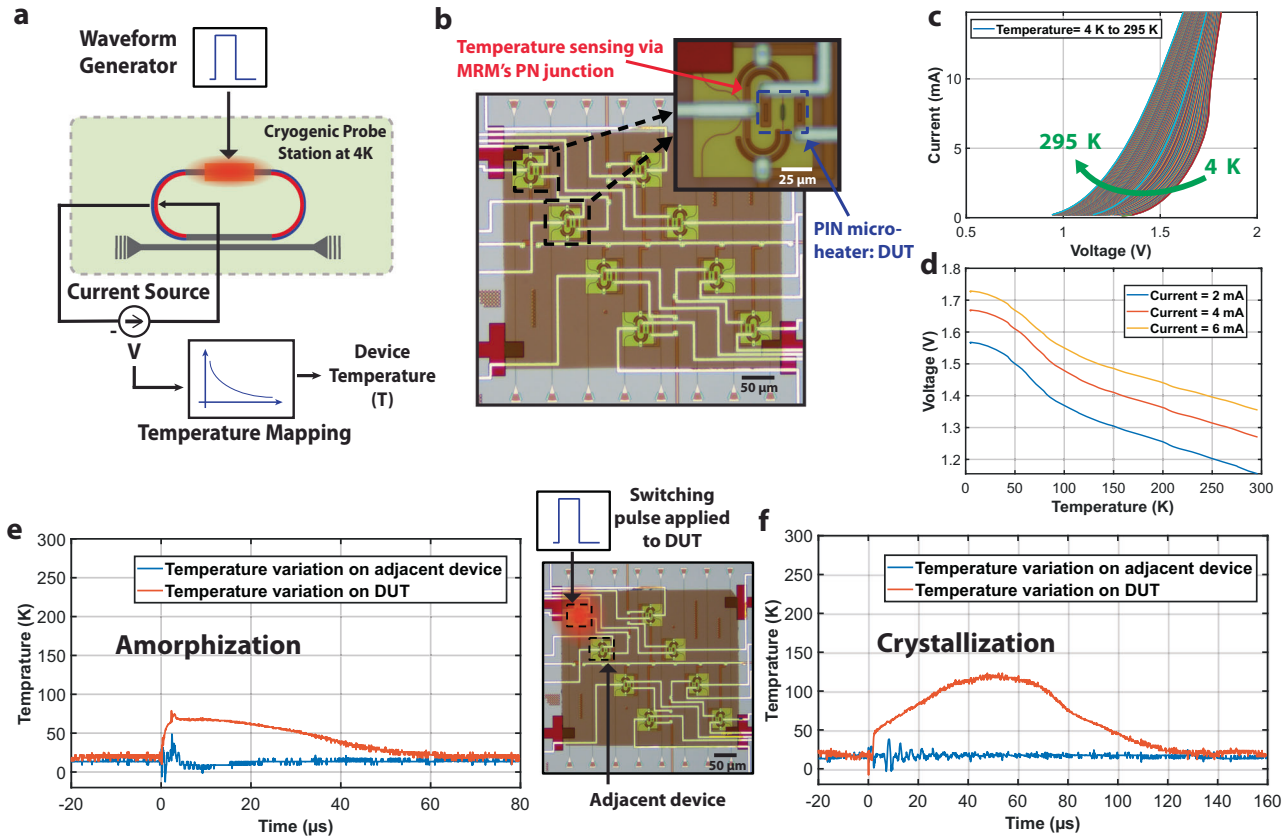

Fig. 3 | Thermal stress characterization. a Schematic of thermal stress characterization setup, **b** Microscope image of the micro-ring modulator (MRM) devices used for thermal stress characterization (PN junctions used as temperature sensors), **c** I-V characteristics of the PN-junctions (temperature sensors) for temperatures from 4 K to 295 K, **d** Voltage across the temperature sensors as a function of temperature. Temperature variations (on device and also on the adjacent device) over time while the amorphization (**e**) or crystallization (**f**) pulse is applied to the device under test (DUT).

After the first partial-amorphization pulse (12 V, 1.15 µs), no eye-opening was observed as there was still a large mismatch between the laser wavelength and resonance, so a second pulse was applied. After the second pulse (12 V, 1.35 µs), a partial eye-opening was detected, prompting the application of a final pulse (12 V, 1.55 µs). With this final amorphization pulse, the maximum eye-opening was achieved by aligning the modulator in its on-resonance state.

Tuning of the resonant modulator to its on-resonance state can be achieved using the non-volatile nature of GST where it self-holds the state with zero static power dissipation once set to a particular state. By starting from the crystalline state, corresponding to the highest λ_{MRM}, and sweeping the resonance to lower wavelengths we ensure that the λ_{MRM} will always be larger than λ_{Laser}. This is critical to avoid any self-heating instability in MRMs[15]. This tuning procedure can be repeated for resonance alignment to any arbitrary laser wavelength within the GST tuning range, with step sizes adjusted according to the resonator's Q-factor and the accuracy of the locking point.

Discussion

We have demonstrated non-volatile tuning of cryogenic resonant modulators using PCM. This approach provides an ideal tuning mechanism to align hundreds of resonators to desired wavelengths with zero static power dissipation, addressing both process variations and thermal drifts. As a result, it enables DWDM optical I/O with aggregate bandwidths in the Tb/s range in a single fiber, supporting ultra-low power and high-speed optical links between 4 K and RT environments for cryogenic classical and quantum computing.

The first-ever non-volatile cryogenic photonic device presented in this work exhibits electrically programmable tuning with high repeatability (see Supplementary Note 2). We observed that the pulse widths required for GST amorphization are ~10× longer at 4 K compared to room temperature, while similar voltage levels are maintained. This behavior is likely due to the cryogenic environment, which facilitates rapid cooling of the melted GST and prevents re-crystallization. Longer amorphization times are advantageous, offering more precise PCM switching to desired states and allowing control over thicker PCM films (see Supplementary Note 3).

Additionally, we characterized the temperature stress around the PIN micro-heater during PCM switching and found no significant temperature rise beyond a 50 µm radius. This ensures that temperature-sensitive devices, such as superconducting nanowire single-photon detectors, can be integrated in close proximity to the proposed resonators without interference. We also demonstrated resonance tuning in a PCM-integrated racetrack MRM, achieving an optical data transmission rate of 10 Gb/s. Although optimizing the electro-optical bandwidths of modulation at 4 K was beyond the scope of this work, it can be improved using higher doping concentrations and optimized junction geometries.

The device was gradually tuned to its on-resonance state through multilevel GST programming at cryogenic temperatures. The current device achieves a tuning range of 0.42 nm, limited by the thickness and length of the GST layer. However, this range could be extended to over 7 nm with minimal impact on the Q-factor by using low-loss PCM such as SbS and SbSe at longer length sections (see Supplementary Note 5). This range is sufficient to cover the FSR of typical MRMs in majority of applications.

https://doi.org/10.1038/s41467-025-64126-2

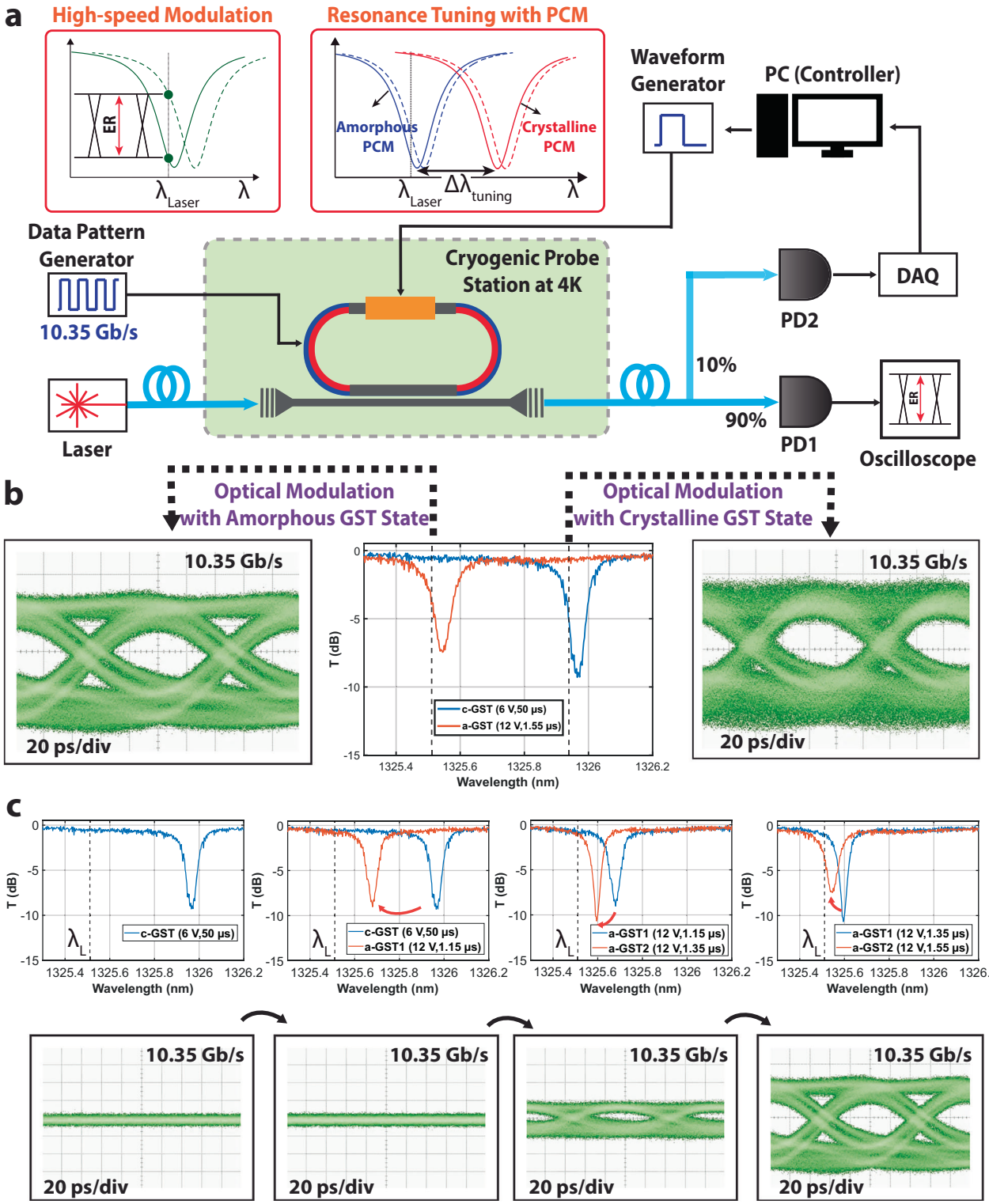

Fig. 4 | Demonstration of resonance tuning in cryogenic silicon photonic micro-ring modulator (MRM). a Block-diagram of the closed-loop resonance tuning using GST programming, **b** High-speed optical data transmission measurements at a-GST on-resonance point and c-GST on-resonance point, **c** Gradual tuning of MRM to its on-resonance state using multilevel GST programming.

While this study focuses on tuning MRMs using cryogenic PCMs, the same method can be used to implement cryogenic optical receivers for WDM operation. Moreover, wide-bandgap, low-loss PCM-based switches can be used to control single-photon paths at cryogenic temperatures, opening up new possibilities for quantum photonics. The non-volatile photonics enabled by PCM in this work can be further extended to cryogenic integrated photonic circuits, featuring thousands of resonant devices operating at ultra-low power with zero static power dissipation, thereby facilitating future applications in quantum technologies, optical and ultra-low-noise computing, and high-energy physics.

Methods

Silicon photonic chip fabrication

We utilized a multi-project wafer (MPW) program to design our silicon photonic chips using the Advanced Micro Foundry (AMF) commercial foundry process. A rib waveguide was implemented in our PIN-micro-heater design to enable single-mode operation in the O-band (1310 nm). We leveraged an existing feature of this technology to open an oxide window down to the silicon layer. While typically used for bio-sensing applications, this method allowed us to deposit the PCM on the desired waveguide sections. A racetrack MRM was designed with a PIN-micro-heater incorporating a 2-μm-wide oxide window opening. Since the oxide etch process at the foundry could potentially damage surrounding metal routings, we ensured that all non-silicon layers, including metal and via layers, were positioned at least 5 μm away from the oxide opening area. This arrangement resulted in a high overall resistance of the micro-heater's parasitic junction.

To achieve low optical losses in the micro-heater, we introduced low doping (n+/p+) in the slab sections near the waveguide core, while increasing the doping concentration further from the core to reduce overall device resistance and maintain low contact resistance at the vias. After receiving the dies from the foundry, each die was post-processed using coarse-resolution lithography for the monolithic integration of GST (see Supplementary Note 1).

Device characterization and testing

We conducted the PCM tuning characterization using an electro-optical cryogenic probe station (Lakeshore CRX-4K). Light was coupled to the resonators via grating couplers, resulting in a loss of 6 dB per coupler at 4 K. Single DC probes were used to contact the electrical terminals of the PIN micro-heater. The test setup included an O-band tunable laser source (Santec TSL-550), power meter (Agilent 81635A), photo-detector (Thorlabs PDB450C), DAQ, source meter (Keithley 2604), and waveform generator (Keysight 33522B). The waveform generator produced the PCM programming pulses. Thermal characterizations were performed by wire-bonding the electrical contacts of the MRM PN junctions to a PCB, using them as temperature sensors. We electrically probed the PIN micro-heater while biasing the temperature sensors (MRM PN junction) with a current source, and recorded voltage variations across them with an oscilloscope.

For high-speed optical data transmission measurements, a bit pattern generator (Keysight N4903A Serial BERT) provided the electrical data input, and the optical output was monitored on an oscilloscope (Keysight 86100D DCA-X) through a high-speed photo-detector (Thorlabs RXM10AF). The high-speed electrical signal was sent to the modulator via RF probes, while single DC probes were used for the PIN micro-heater (see Supplementary Fig. S3). We measured the ER and IL by directly observing the optical power on an optical scope. An additional PD was employed to monitor and sense the optical power inside the resonator. The PD output was digitized and read by a data acquisition (DAQ) unit, which sent the data to a PC controller. The controller processed the data to continuously tune the GST state and adjust λ_{MRM}, bringing it close to λ_{Laser}.

Data availability

The data underlying the findings of this study are included in the article and its supplementary information. Additional data are available from the corresponding author upon request.

References

1. Lecocq, F. et al. Control and readout of a superconducting qubit using a photonic link. *Nature* **591**, 575–579 (2021).
2. Abi, B. et al. *Deep Underground Neutrino Experiment (DUNE), Far Detector Technical Design Report, Volume II: DUNE Physics*, 2 (IOP Science, 2020).
3. Magnard, P. et al. Microwave quantum link between superconducting circuits housed in spatially separated cryogenic systems. *Phys. Rev. Lett.* **125**, 260502 (2020).
4. Reilly, D.J. Challenges in scaling-up the control interface of a quantum computer. In *2019 IEEE International Electron Devices Meeting (IEDM)*, 31–7 (IEEE, 2019).
5. Youssefi, A. et al. A cryogenic electro-optic interconnect for superconducting devices. *Nat. Electron.* **4**, 326–332 (2021).
6. Gevorgyan, H. et al. Cryo-compatible, silicon spoked-ring modulator in a 45nm cmos platform for 4k-to-room-temperature optical links. In *2021 Optical Fiber Communications Conference and Exhibition (OFC)*, 1–3 (IEEE, 2021).
7. Pintus, P. et al. Ultralow voltage, high-speed, and energy-efficient cryogenic electro-optic modulator. *Optica* **9**, 1176–1182 (2022).
8. Gehl, M. et al. Operation of high-speed silicon photonic micro-disk modulators at cryogenic temperatures. *Optica* **4**, 374–382 (2017).
9. Mirhosseini, M., Sipahigil, A., Kalaee, M. & Painter, O. Superconducting qubit to optical photon transduction. *Nature* **588**, 599–603 (2020).
10. Weaver, M. J. et al. An integrated microwave-to-optics interface for scalable quantum computing. *Nat. Nanotechnol.* **19**, 166–172 (2024).
11. Rakowski, M. et al. 45nm cmos-silicon photonics monolithic technology (45clo) for next-generation, low power and high speed optical interconnects. In *Optical Fiber Communication Conference*, T3H–3 (Optica Publishing Group, 2020).
12. Siew, S. Y. et al. Review of silicon photonics technology and platform development. *J. Lightwave Technol.* **39**, 4374–4389 (2021).
13. Pernice, W. H. P., Schuck, C., Li, M. & Tang, H. X. Carrier and thermal dynamics of silicon photonic resonators at cryogenic temperatures. *Opt. Express* **19**, 3290–3296 (2011).
14. Dong, P. et al. Thermally tunable silicon racetrack resonators with ultralow tuning power. *Opt. Express* **18**, 20298–20304 (2010).
15. Moazeni, S. et al. A 40-Gb/s PAM-4 transmitter based on a ring-resonator optical DAC in 45-nm SOI CMOS. *IEEE J. Solid-State Circuits* **52**, 3503–3516 (2017).
16. Atabaki, A. H. et al. Integrating photonics with silicon nanoelectronics for the next generation of systems on a chip. *Nature* **556**, 349–353 (2018).
17. Sun, C. et al. Single-chip microprocessor that communicates directly using light. *Nature* **528**, 534–538 (2015).
18. Komma, J., Schwarz, C., Hofmann, G., Heinert, D. & Nawrodt, R. Thermo-optic coefficient of silicon at 1550 nm and cryogenic temperatures. *Appl. Phys. Lett.* **101**, 041905 (2012).
19. Estrella, S. B., Dorch, T. P., Cooper, T. M., Renner, D. S. & Schow, C. L. Novel link architecture minimizing thermal energy dissipation for cryogenic optical interconnects. In *Optical Fiber Communication Conference*, F2E–3 (Optica Publishing Group, 2021).
20. Dong, M. et al. High-speed programmable photonic circuits in a cryogenically compatible, visible-near-infrared 200mm CMOS architecture. *Nat. Photonics* **16**, 59–65 (2022).
21. Pintus, P. et al. An integrated magneto-optic modulator for cryogenic applications. *Nat. Electron.* **5**, 604–610 (2022).
22. Shen, M. et al. Photonic link from single-flux-quantum circuits to room temperature. *Nat. Photonics* **18**, 371–378 (2024).
23. Eltes, F. et al. An integrated optical modulator operating at cryogenic temperatures. *Nat. Mater.* **19**, 1164–1168 (2020).
24. Han, H. et al. Cryogenic photonic readout based on thin-film lithium niobate mach–zehnder modulators. *IEEE Photonics J.*, **16**, 7201305 (2024).
25. Chakraborty, U. et al. Cryogenic operation of silicon photonic modulators based on the dc kerr effect. *Optica* **7**, 1385–1390 (2020).
26. Gyger, S. et al. Reconfigurable photonics with on-chip single-photon detectors. *Nat. Commun.* **12**, 1408 (2021).

27. Fang, Z., Chen, R., Zheng, J. & Majumdar, A. Non-volatile reconfigurable silicon photonics based on phase-change materials. *IEEE J. Sel. Top. Quantum Electron.* **28**, 1–17 (2021).
28. Chen, R. et al. Opportunities and challenges for large-scale phase-change material integrated electro-photonics. *ACS Photonics* **9**, 3181–3195 (2022).
29. Xu, P., Zheng, J., Doylend, J. K. & Majumdar, A. Low-loss and broadband nonvolatile phase-change directional coupler switches. *ACS Photonics* **6**, 553–557 (2019).
30. Zhou, W. et al. In-memory photonic dot-product engine with electrically programmable weight banks. *Nat. Commun.* **14**, 2887 (2023).
31. Shastri, B. J. et al. Photonics for artificial intelligence and neuromorphic computing. *Nat. Photonics* **15**, 102–114 (2021).
32. Zheng, J. et al. Gst-on-silicon hybrid nanophotonic integrated circuits: a non-volatile quasi-continuously reprogrammable platform. *Optical Mater. Express* **8**, 1551–1561 (2018).
33. Zheng, J. et al. Nonvolatile electrically reconfigurable integrated photonic switch enabled by a silicon pin diode heater. *Adv. Mater.* **32**, 2001218 (2020).
34. Chen, R. et al. Broadband nonvolatile electrically controlled programmable units in silicon photonics. *ACS Photonics* **9**, 2142–2150 (2022).
35. Delaney, M., Zeimpekis, I., Lawson, D., Hewak, D. W. & Muskens, O. L. A new family of ultralow loss reversible phase-change materials for photonic integrated circuits: Sb_2S_3 and Sb_2Se_3. *Adv. Funct. Mater.* **30**, 2002447 (2020).
36. Chen, R. et al. Non-volatile electrically programmable integrated photonics with a 5-bit operation. *Nat. Commun.* **14**, 3465 (2023).
37. Ríos, C. et al. Ultra-compact nonvolatile phase shifter based on electrically reprogrammable transparent phase change materials. *PhotoniX* **3**, 26 (2022).
38. Wu, C. et al. Freeform direct-write and rewritable photonic integrated circuits in phase-change thin films. *Sci. Adv.* **10**, eadk1361 (2024).
39. Fang, Z. et al. Arbitrary programming of racetrack resonators using low-loss phase-change material Sb_2Se_3. *Nano Lett.* **24**, 97–103 (2023).
40. Fang, Z. et al. Ultra-low-energy programmable non-volatile silicon photonics based on phase-change materials with graphene heaters. *Nat. Nanotechnol.* **17**, 842–848 (2022).
41. Erickson, J. R., Shah, V., Wan, Q., Youngblood, N. & Xiong, F. Designing fast and efficient electrically driven phase change photonics using foundry compatible waveguide-integrated microheaters. *Opt. Express* **30**, 13673–13689 (2022).
42. Erickson, J. R. et al. Comparing the thermal performance and endurance of resistive and pin silicon microheaters for phase-change photonic applications. *Optical Mater. Express* **13**, 1677–1688 (2023).
43. Wuttig, M., Bhaskaran, H. & Taubner, T. Phase-change materials for non-volatile photonic applications. *Nat. photonics* **11**, 465–476 (2017).
44. Park, J., Kim, M. R., Choi, W. S., Seo, H. & Yeon, C. Characterization of amorphous phases of ge2sb2te5 phase-change optical recording material on their crystallization behavior. *Jpn. J. Appl. Phys.* **38**, 4775 (1999).
45. Morales-Sanchez, E., Prokhorov, E. F., Mendoza-Galván, A. & González-Hernández, J. Determination of the glass transition and nucleation temperatures in ge 2 sb 2 te 5 sputtered films. *J. Appl. Phys.* **91**, 697–702 (2002).
46. Orava, J., Greer, A. L., Gholipour, B., Hewak, D. W. & Smith, C. E. Characterization of supercooled liquid ge2sb2te5 and its crystallization by ultrafast-heating calorimetry. *Nat. Mater.* **11**, 279–283 (2012).
47. Wu, C., Sturm, D., Adya, U., Li, M. & Moazeni, S. Integration of phase change material with commercial 45nm monolithic silicon photonics. In *CLEO: Science and Innovations*, SF3E–5 (Optica Publishing Group, 2023).
48. Wei, M. et al. Monolithic back-end-of-line integration of phase change materials into foundry-manufactured silicon photonics. *Nat. Commun.* **15**, 2786 (2024).
49. Chen, R. et al. Deterministic quasi-continuous tuning of phase-change material integrated on a high-volume 300-mm silicon photonics platform. *npj Nanophotonics* **1**, 7 (2024).
50. Adya, U. et al. Post-processing of phase change material in a zero-change commercial silicon photonic process. *Opt. Express* **32**, 27552–27562 (2024).
51. Charbon, E. et al. Cryo-CMOS for quantum computing. In *2016 IEEE International Electron Devices Meeting (IEDM)*, 13.5.1–13.5.4, (IEEE, 2016).
52. Gui, H. et al. Review of power electronics components at cryogenic temperatures. *IEEE Trans. Power Electron.* **35**, 5144–5156 (2020).
53. Kari, S. R. et al. High-speed multifunctional photonic memory on a foundry-processed photonic platform. *Optica* **12**, 31–38 (2025).
54. Yuan, Y. et al. A 100 gb/s pam4 two-segment silicon microring resonator modulator using a standard foundry process. *ACS Photonics* **9**, 1165–1171 (2022).
55. Rakowski, M. et al. 45nm CMOS - Silicon photonics monolithic technology (45CLO) for next-generation, low power and high speed optical interconnects. In *Optics InfoBase Conference Papers*, volume Part F174, (IEEE, 2020).

Acknowledgements

We would like to acknowledge CMC Microsystems for providing MPW fabrication services for AMF Silicon Photonics technology. Post-processing steps were conducted at the Washington Nanofabrication Facility (WNF), a National Nanotechnology Coordinated Infrastructure (NNCI) site at the University of Washington, with partial support from the National Science Foundation via awards NNCI-1542101 and NNCI-2025489. This work is supported by National Science Foundation (NSF) under Grant No. CCF-2105972, the U.S. Department of Energy (DOE) under Award Number DE-SC0024729, and ONR MURI (award no. N00014-17-1-2661). A.M and R.C. are supported by NSF-FuSe Award Number 2329089.

Author contributions

U.A. and S.M. conceived the idea. U.A. designed, modeled, and fabricated the devices, conducted the experiments, and analyzed the data. S.S. assisted with the experiments, data analysis, and modeling of devices. R.C. contributed to the fabrication of the devices. I.T. and S.J. contributed to the preparation of the test experiment setup. S.M., M.L., and A.M. supervised the project. S.M. directed the project, and U.A. and S.S. wrote the manuscript with contributions from all authors.

Competing interests

The authors declare no competing interests.

Additional information

Supplementary information The online version contains supplementary material available at https://doi.org/10.1038/s41467-025-64126-2.

Correspondence and requests for materials should be addressed to Sajjad Moazeni.

Peer review information *Nature Communications* thanks the anonymous reviewer(s) for their contribution to the peer review of this work. A peer review file is available.